Baku State University: Journal of Physics & Space Sciences, **2025**, v 2 (1), p. 19-41

journal homepage: http://bsuj.bsu.edu.az/en

Structural characteristics of the heme-containing domain complex of soluble guanylate cyclase with carnosine based on molecular modeling methods

Svetlana D. Demukhamedova[1], Irada N. Aliyeva[*2]

[1]Scientific Research Institute for Physics Problems, Baku State University, Baku, Azerbaijan,
[2]Department of Optics and Molecular Physics, Baku State University, Baku, Azerbaijan,
Received 10-Jan-2025; Accepted 12-Feb-2025
DOI: https://doi.org/10.30546/209501.101.2025.2.300.07

Abstract

The structure of the tautomeric form N^1H of carnosine (β −alanine−L − histidine) complex with the active site of soluble guanylate cyclase was investigated based on molecular mechanics, quantum chemistry, and molecular docking methods. It was shown that carnosine binding occurs in a region close to the heme pocket of guanylate cyclase and is characterized by a binding affinity of about −4.5 kcal/mol. The obtained results may be useful for predicting and using carnosine and its analogues as inhibitors of soluble guanylate cyclase for the development of new therapeutic drugs.

Keywords: carnosine, soluble guanylate cyclase, quantum−chemical calculations, molecular modeling methods.
PACS: 87.15 Aa, 87.15.He, 87.15.By

1. Introduction

Modern achievements in the field of molecular modeling of biological systems are based on theoretical research that use various approximations of non-empirical and semi-empirical quantum chemistry methods, allowing for description and an adequate interpretation of the relationship between the geometrical, electron and chemical structure of molecular complexes. To date, there are a large number of

[*]*Corresponding author*. Tel.: (+994) 55 703 65 45
e-mail: aliyeva.irada.bsu23@gmail.com; ORCID ID: 0000-0002-5400-6198.

computational programs based on such methods and widely used for the calculation of geometrical, thermodynamical, and spectroscopical parameters of molecules and the investigation of their chemical reactivity. Well- known theoretical methods of molecular mechanics, molecular dynamics, and molecular docking describe not only the static and dynamic properties of molecules but also give an opportunity for the optimization of the ligand's position within the active center of protein molecules. Based on the results of quantitative calculations of protein-ligand interaction energies, it is possible to study the structure of the stable complex, investigate conformational transitions, and analyze parameters that characterize the peculiarities of complex formation processes. In most cases, integrated approaches based on a combination of experimental data and theoretical calculations are the most informative in solving structural-functional relationships of proteins and their complexes. Such approaches allow for quantitative calculations and provide the opportunity not only to visually observe the processes of dynamic transformations but also to predict the optimal pathways for implementing the complex formation processes of complex biological systems. Molecular modeling methods are a highly effective tool for scientific research among a wide range of tasks and open new possibilities for the targeted synthesis of pharmaceuticals with a prepredictable spectrum of their functional activity. The most common and convenient modern software packages for researchers in molecular modeling are Gaussian, HyperChem, GaussView, PyMol, AutoDockTools, and others [1-3]. Based on such computational programs the spatial and electronic structure of a big number of natural compounds—peptides, proteins, polymers, and their complexes with transition metals, as well as newly synthesized chemical compounds with a wide range of functional and optical activities, ligand-receptor interactions have been studied.

In this work the electronic and spatial structure of the heme-containing region of the catalytic domain of soluble guanylate cyclase with the carnosine molecule, which acts as a ligand in protein inhibition processes has been studied. Investigations were carried out by the semi-empirical quantum chemistry method PM3 and non-empirical calculations based on the density functional theory (DFT) with the hybrid B3LYP potential using the 6-31+G(d,p) basis set. Molecular docking including step-by-step modeling of the binding process between carnosine and active site of the titled protein are described in detail. It is known that soluble guanylate cyclase is present in most types of mammalian cells and demonstrates a wide range of important physiological functions, such as inhibition of platelet aggregation, relaxation of smooth muscles, vasodilation, regulation of the gastrointestinal system, neuronal signal transduction, and immunomodulation. Deviations in guanylate cyclase activity lead to numerous pathological disorders [4-10]. Experiments showed that guanylate cyclase can be activated by nitric oxide, which binds to the heme-containing site of the protein and participated in the regulation of the cardiovascular, nervous, and gastrointestinal systems of the body [11-13].

Soluble guanylate cyclase (sGC) is a heterodimer consisting of α and β subunits [14-20]. The subunits exist in various isoforms, α1, α2, β1, abd β2, but the most common subunits are α1 and β1 [21]. Both subunits are necessary for protein activation (Fig. 1).

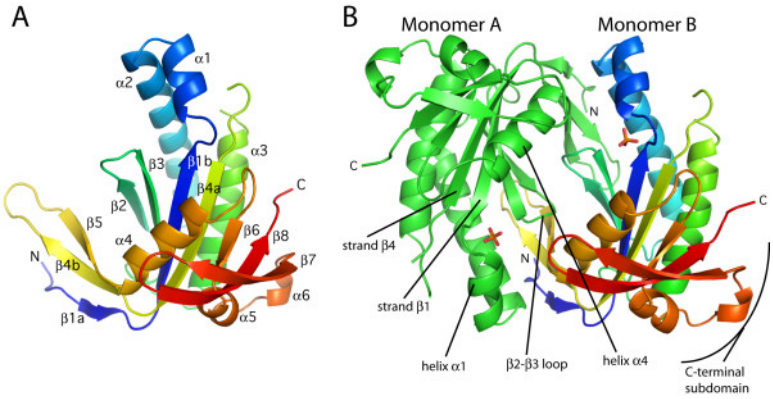

Fig. 1. Structure of soluble guanylate cyclase [14-20].

Each sGC subunit consists of 4 domains: the N-terminal sensor domain H-NOX, a PAS-like domain, a coiled-coil domain, and the C-terminal catalytic domain (Fig. 2) [14, 15].

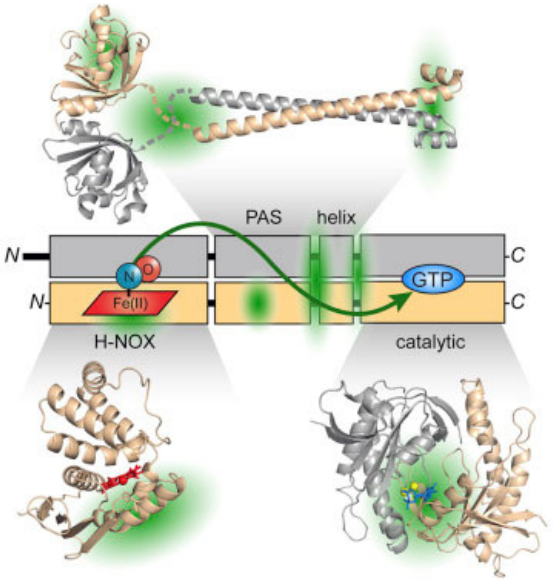

Fig. 2. Structural domains of soluble guanylate cyclase corresponding to conformational changes induced by nitric oxide binding [22-25].

It is known that determining the three-dimensional structure of membrane proteins is a very difficult problem related to the isolation of the protein in pure form from the lipid environment. Since the ligand-binding domain of guanylate cyclase is located on the surface of cell membranes, it was possible to determine the structure of this part of the protein responsible for ligand binding. The protein molecule penetrates the membrane in such a way that it consists of three spatially separated parts:

- external ligand-binding site located on the outer side of the membrane;
- transmembrane segment, penetrating the lipid bilayer;
- cytoplasmic part.

In the cytoplasmic domain, a sequence homologous to the sequence of soluble GC and protein kinase was found; the C-terminal sequence of guanylate cyclase is very hydrophobic but rich in serine residues, which can be considered as potential phosphorylation acceptors. The amino acid sequence of the extracellular domain of sGC, which includes a hydrophilic N-terminal fragment, was synthesized using genetic engineering methods, crystallized in a free state, and studied with resolution in 3.8 Å [16]. The guanylate cyclase also includes a heme-containing domain, participating in binding nitric oxide.

Studies on guanylate cyclase activity have shown that the binding of the heme-containing enzyme soluble guanylate cyclase (sGC) with a nitric oxide (NO) molecule leads to a 200-fold increase in guanylate cyclase activity and raises the level of cyclic guanosine monophosphate (cGMP), which is one of the important mediators of intracellular signal transduction (Fig. 2) [24-36]. However, it is also known that NO and its derivatives are involved in pathogenic processes in various types of diseases, including neurodegenerative disorders. In the case of excessive NO formation, diseases such as Parkinson's disease, asthma, migraine, cancer, sepsis, and septic shock are observed [37-45]. There is a need to develop drugs that are inhibitors of NO-dependent guanylate cyclase activation at its elevated concentration in the body.

One such inhibitor is the carnosine molecule, a small natural molecule containing two amino acid residues, β −alanine and L −histidine [46-62]. It has been suggested that carnosine exerts an inhibitory effect on the guanylate cyclase activation due to the interaction of carnosine with Fe^{2+}, which is part of the heme component of sGC. It inhibits the activation of the enzyme by NO donors but does not affect the stimulation of guanylate cyclase by compounds that do not generate NO. Carnosine and its derivatives, partially homocarnosine (gamma-aminobutyryl−L −histidine) and anserine (N −methyl carnosine), prevent and reduce such pathologies as amyotrophic lateral sclerosis and the most common neurodegenerative diseases—Alzheimer's and Parkinson's diseases.

In this regard, new prospects are opening up for the development of new drugs with a predictable effect based on carnosine and its analogues associated with the

enhancement of the intracellular NO–sGC signaling system. The study of the structural peculiarities of carnosine, as well as the spatial and electronic characteristics of the complex upon its selective binding to the active site of NO-dependent guanylate cyclase, is the main objective of this research.

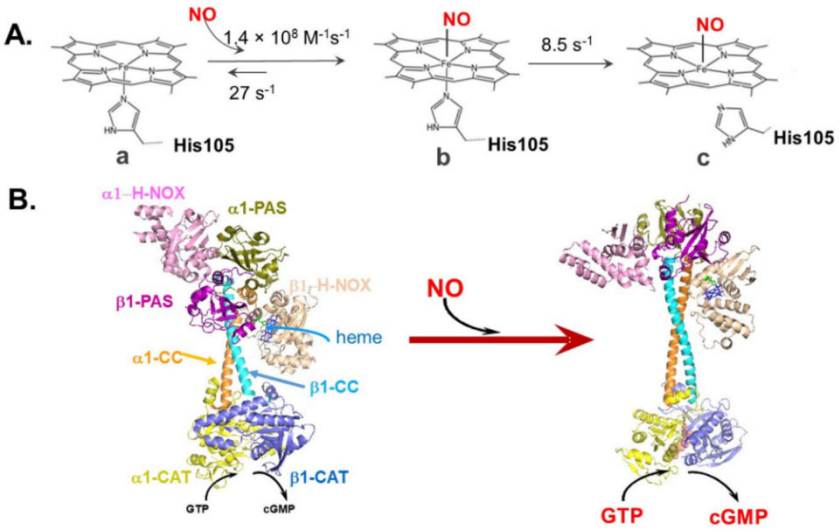

Fig. 2. (A) The heme component of soluble guanylate cyclase involved in nitric oxide binding; (B) Structural rearrangement of sGC domains [23].

In a number of our works, the structures and electronic characteristics of free carnosine and its derivatives-homocarnosine and anserine-were thoroughly investigated in gas and aqueous medium [63-66]. Theoretical methods of molecular mechanics using the MM+ force field and the semi-empirical quantum chemistry method PM3 were employed to establish the low-energy conformational states of these compounds, calculate the values of partial charges, study the distribution of electronic density, and conduct a comparative analysis of the obtained results. It was found that the folded conformational states of the dipeptides are more stable compared to other structures, and the distribution of charge electronic density confirms the conclusions that the molecule and its derivatives possess a pronounced ability to perform proton buffer functions.

Thus, using the results of our previous works, this study is dedicated to modeling the complexation processes of the heme-containing fragment of the soluble guanylate cyclase catalytic domain with the tautomeric form of N^1H carnosine. Based on molecular docking and the analysis of the results of the carried out calculations, the structural and energetic characteristics of the optimized complex structures are described.

2. Research methods

As noted above, this work is based on results of previously carried out investigations [63-66], in which the descriptors of the reactivity of the free carnosine molecule were studied, charges on atoms were calculated, dipole moment values, HOMO and LUMO energies were determined, atomic orbital occupancy was analyzed, molecular electrostatic potential distribution maps were constructed, and the donor-acceptor properties of individual atoms and functional groups of carnosine were analyzed. Both molecular mechanics methods and semi-empirical and non-empirical quantum-chemical calculations were used in this work. In the MM+ molecular mechanics method, semi-empirical field potentials were used with the Polak-Ribiere algorithm at an accuracy of 0.001 kcal/mol. The data obtained using the MM+ method were chosen as the basis for calculations with the semi-empirical quantum chemistry method PM3, specifically parameterized for transition metal atoms. Within the framework of this method, the geometric structure was refined by its optimization using the conjugate gradient method with a step size 0.1 kkal /Å ·mol and a varying number of iterations until convergence was achieved. The equilibrium geometric configuration of the carnosine molecule was established based on the search for the global minimum of the total energy as a function of the geometric configuration of the atomic nuclei and the establishment of stationary points on multidimensional potential surfaces according to the data from our previous studies. The total energy of the molecular system is represented as the additive sum of different types of interactions, such as non-valent, electrostatic, torsional, bond length and valence angle deformation energies, and hydrogen bond formation energy. Based on the calculation results, a detailed analysis of the occupancy of atomic orbitals was conducted, and the charge transfer in complexation processes was schematically shown. For the calculation of charge distribution, the Mulliken model was used. The influence of conformational mobility on the geometric parameters and the distribution of electronic density on the atoms of various functional groups in the complex was studied. Calculations were performed using the Gaussian 09 programs pack [1]. To visualize the obtained results, the program GaussView 6.0.16 [2] was used. For the calculations of molecules, the density functional theory method with the hybrid potential B3LYP and the 6-31+G(d,p) basis set was used.

Among the split-valence basis sets, the extended basis 6-31+G(d,p) is widely used. In this basis set the core orbitals are composed of six Gaussian functions, and the valence electron orbitals are divided into two components. The first of these basis functions is composed of three Gaussian functions, while the second consists of a single uncontracted Gaussian primitive. In the split-valence basis set 6-31+G(d,p), the contraction of valence orbitals is taken into account. The average errors in the bond lengths and valence angles were found to be approximately 1%,

while the average error for electronic density was found to be 10%. The average error for the energy of conformational transitions (rotation and inversion barriers) was found to be ≤ 2 kcal/mol.

In this study, molecular docking was used to investigate the binding processes of carnosine with the heme site of the soluble guanylate cyclase. Molecular docking is a method of molecular computer simulating the molecular recognition process. The docking procedure is used at the early stages of drug development and prediction, and it is one of the most crucial stages of this process. It aims to achieve an optimized relative positions for both the protein and ligand such that the free energy of the complex system is minimized. Different types of non-covalent interactions, such as van der Waals, coulombic, torsion, hydrogen bondings and others cause the protein and small ligand molecule to bind together to form a stable complex.

AutoDockTools version 1.5.6 [67] was used to predict the interaction between ligand and active site of soluble guanylate cyclase protein. The molecular docking software also allows to analyze the docking experiment. It includes tools for preparing input files, visualizing the calculation results and analyzing the predicted binding modes. The protein structure is prepared by removing crystallographic water molecules, adding hydrogen atoms that are missing in the X-ray structure, and assigning partial charges to the protein atoms. The preparation of the ligand includes adding Gasteiger charges to the ligand atoms and determining its torsional rotation angles. After such a preparation procedure, the protein and ligand files are saved in .pdbqt format. Next, to determine the space in which the ligand-protein interaction modeling will take place, a hypothetical box-cube with a side length of 10-30 Å, including the active site of the protein, is selected. Using AutoGrid, a set of potential grids is created for the protein, describing the interaction potential for each atom within the hypothetical "box" with a probe atom of a specific chemical element. Inside the box, the ligand moves and rotates. Autodock iterates through all possible positions and conformations of the ligand within the "box" to find positions with the best binding energy. Then a configuration file is saved, and the program proceeds directly to docking. The modeling of the ligand docking process with the rigid structure of the protein was conducted using the AutoDoc Vina program [68]. The semi-empirical formula of the free energy of the force field, with which AutoDock evaluates the interaction energy of atoms, contains both terms corresponding to molecular-mechanical interactions and empirical terms assessing the interaction with water. The free energy of interaction is assumed to be equal to the difference between the sum of the energies of the ligand and the protein in the separated unbound state and the energy of the ligand-protein complex. The free energy formula includes 6 terms corresponding to all possible pairwise interactions and the estimation of conformational entropy loss upon binding:

$$\Delta G = \left(V_{bound}^{L-L} - V_{unbound}^{L-L}\right) + \left(V_{bound}^{P-P} - V_{unbound}^{P-P}\right) +$$

$$\left(V_{bound}^{P-L} - V_{unbound}^{P-L} + \Delta S_{conf}\right),$$

where $L -$ ligand and $P -$ protein.The first bracket corresponds to the difference in intramolecular energy of the ligand in the bound and unbound conformations with the protein, the second is the change in intramolecular energy of the protein, and the third is the change in intermolecular energy. The paired terms V contain estimates of Van der Waals interaction forces (6/12 potential, parameters A and B from the AMBER force field), hydrogen bonds (10/12 potential), electrostatics, and solvation energy:

$$V = W_{vdw} \sum_{ij} \left(\frac{A_{ij}}{r_{ij}^{12}} - \frac{B_{ij}}{r_{ij}^{6}}\right) + W_{hbond} \sum_{ij} E(t) \left(\frac{C_{ij}}{r_{ij}^{12}} - \frac{D_{ij}}{r_{ij}^{10}}\right) +$$

$$W_{elec} \sum_{ij} \frac{q_i q_j}{e(r_{ij}) r_{ij}} + W_{sol} \sum_{ij} (S_i V_j - S_j V_i) e^{(-r_{ij}^2/2\sigma^2)}$$

The weighting coefficients are selected to minimize the difference between the binding energy estimate and the experimental data. For the visualization and analysis of ligand-enzyme interactions in 3D, we used the molecular graphics system PyMol, version 1.7.x [3].

3. Results and discussion

A truncated model of guanylate cyclase was chosen in this study. The structural pdb files of the signaling protein molecule of soluble guanylate cyclase used in this work were obtained from the Protein Data Bank at http://www.rcsb.org (pdb code 1xbn). Fig. 3 shows the initial model of the structure of soluble guanylate cyclase pdb.1xbn in complex with heme, located in the protein's binding pocket.

Quantum-chemical analysis. Reactivity descriptors

To study the structural changes and electronic characteristics of the active site of the protein responsible for ligand binding, a region located around the heme at a distance of 4 Å is selected. This procedure allows us to see all the side chains in this region of the protein corresponding to the amino acid residues in the primary structure of the protein. In Fig.4, the names of the amino acid residues whose side chains participate in non-covalent interactions with its heme component are indicated. From the presented figure, it can be seen that the Fe^{2+} atom of the heme is in close proximity to the imidazole ring of His 102.

As seen in Fig.4, in the structure of the protein pdb.1xbn with a resolution of 2.5 Å from the Protein Data Bank (https://www.rcsb.org/) according to the work [69], the heme pocket is wedged between two domains. On one side of the heme, its

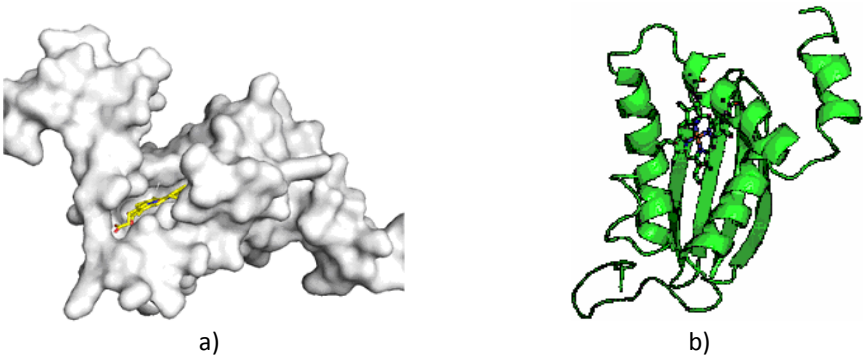

a) b)

c)

Fig. 3. Structure of the guanylate cyclase protein (pdb.1xbn) with the heme located in the enzyme's "pocket." (a), (b), and (c) correspond to different images of the same spatial structure.

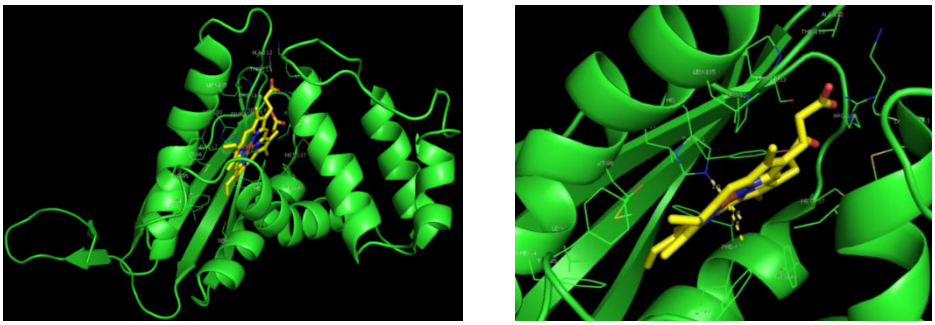

a) b)

Fig. 4. Active site region of guanylate cyclase protein indicating amino acid residues (a) and (b) with the imidazole ring His 102 located near the heme according to [69].

iron atom is coordinated with the imidazole ring of the amino acid residue His102. On the other side of the heme, due to the interaction of the heme iron atom with the oxygen atoms of another ligand in the 1xbn-O_2 structure, two more coordination bonds are formed between the heme iron and the oxygens. The length of the Fe-N bond with His 102 is 2.0 Å, while the lengths of the bonds with $Fe - O_1$ and $Fe - O_2$ are 2.8 Å and 1.8 Å, respectively. The propionic acid residues of the heme are linked by hydrogen bonds to the side chains of Tyr131, Ser133, and Arg135. Between the tetrapyrrole and the residues that form the binding pocket, there are numerous non-bonded contacts. The distal pocket of the heme is nonpolar, except

for Tyr140, and there are no polar atoms in the heme itself. The side chain of the amino acid Tyr139 in the distal pocket modulates the strength of the proximal Fe-His bond. The N^1H tautomer of free carnosine was chosen as a ligand molecule for the docking procedure. Fig.5 shows the stable conformational state of the carnosine dipeptide molecule in the tautomeric form of its imidazole ring (N^1H) corresponding to the minimum value of the total conformational energy. The methodology for calculating and analyzing the conformational mobility of the natural dipeptide was described in detail in the works [63-66].

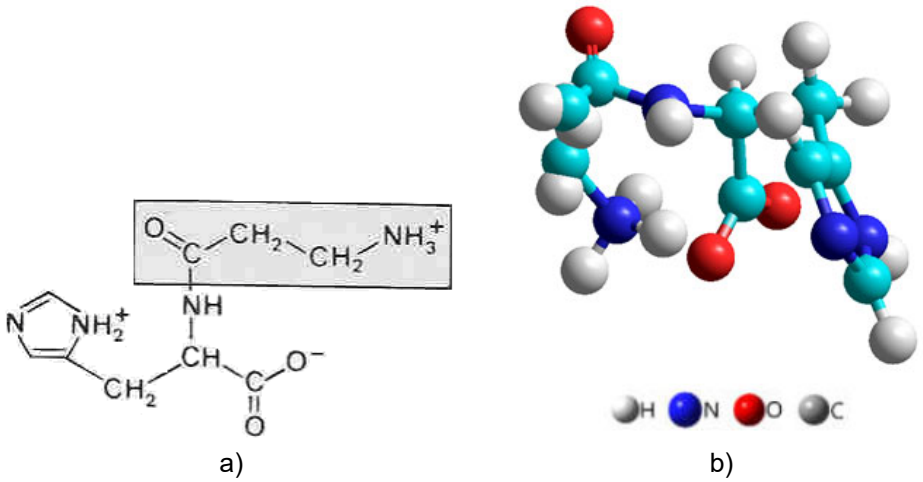

Fig. 5. (a) Model of the carnosine molecule in the tautomers form N^1H and (b) low-energy conformational state according to [28].

Table 1 presents the main energy and electron characteristics of the carnosine molecule obtained from the conducted studies [63-66]. In the most stable conformation of carnosine, the interatomic distances between the nitrogen atom of the α-amino group and the oxygen atoms of its deprotonated carboxyl group NH (His)…-OOC is 2.9 Å. The formation of a hydrogen bond is characteristic of the hydrogen atom of the amide group of the main chain His and the oxygen atoms of the COO^- group (bond length is 1.95 Å, hydrogen bond energy is -1.30 kcal/mol).

The analysis of frontier molecular orbitals, due to their highest availability for electrophiles and nucleophiles, allows for the study of the chemical reactivity of carnosine. By the sign of the energy of the lowest unoccupied molecular orbital (LUMO) of the molecule, it is possible to determine whether it belongs to electrophilic or nucleophilic reagents. If the LUMO energy is positive, the molecule is classified as a nucleophile; if it is negative, as an electrophile. According to our calculations, the molecule of carnosine is conditionally classified as an electrophile. The energy gap between the orbitals of the ground (HOMO) and excited (LUMO) states

provides useful information about the stability of the structure. The smaller the energy gap, the higher the chemical and biological activity of the studied compound (Table 1). Mathematically, global descriptors can be obtained from the energy values of frontier orbitals, providing comprehensive chemical information about molecular structure, correlating with specific properties of molecules, and proving useful in solving various pharmacological, chemical, and toxicological problems. According to the Koopmans' theorem, the first ionization energy is equal to the negative value of the HOMO: $I = -E_{HOMO}$. And the electron affinity is defined as the negative value of the LUMO: $A = -E_{LUMO}$. Based on these values, important indices for predicting the reactivity of a molecule, such as electronegativity $\chi = (I + A)/2$, chemical potential $\mu = -(I + A)/2$, chemical hardness $\eta = (I - A)/2$, and softness $S = 1/2\eta$, can be calculated. The electrophilicity index $\omega = \mu^2/2\eta$ indicates the ability of a molecule to accept electrons from a reagent, while the opposite value is the nucleophilicity index $\nu = 1/\omega$. An important global descriptor is the maximum charge transfer $\Delta N = -\mu/\eta$ that an electrophilic system can accept [70-81]. The calculated descriptors of the reactivity of carnosine are presented in Table 1.

Table 1. The reactivity descriptors and electronic parameters of the optimized structure of the carnosine molecule

Physical quantities	**Parameter values (eV)**
Electronic energy	-110817.41
E_{HOMO}	-6.649377
E_{LUMO}	-0.437287
Energy gap ΔE	6.212090
Ionization potential $I = -E_{HOMO}$	6.649378
Electron affinity $A = -E_{LUMO}$	0.437287
Electronegativity χ=(I+A)/2	3.543332
Chemical potential μ= -(I+A)/2	-3.543332
Global hardness η=(I-A)/2	3.106045
Softness S=1/2η	0.321953
Electrophilicity index ω=μ^2/2η	2.021092
Nucleophilicity (**ν**)	0.494782
Maximum charge transfer (ΔN)	1.140786
Polarizability (α)	3924.134026
Dipole moment (debye)	6.4

The Mulliken charges on the atoms of the carnosine molecule obtained as a result of optimization using the PM3 method were presented in Table 2. It is well

known that Mulliken charges do not reflect the actual distribution of electric charge between atoms and are quite sensitive to the choice of basis set. However, they are convenient for a qualitative assessment of charge distribution and for identifying electrophilic and nucleophilic centers of possible attacks.

Table 2. Partial charges on the atoms of the carnosine molecule (in units of electron charge)

Carnosine	Aliphatic chain							Carboxyl group			Imidazole ring					
Atom	C1	C2	C3	N4	O6	N5	C7	C8	O9	O10	C11	C12	C13	N15	N14	C16
Charge	0.352	-0.061	0.122	-0.202	-0.328	-0.219	0.075	0.383	-0.257	-0.327	0.001	0.037	0.028	-0.199	-0.078	0.139

With the help of molecular modeling programs, it is possible to obtain a convenient three-dimensional visualization of the electronic properties of the studied compounds. Fig.6 shows the HOMO, LUMO energies and their difference for the carnosine molecule. The areas of electronic transitions between the molecular orbitals are easily visible. The red color in the figure indicates the presence of electrons (area with negative charge), while the green color indicates the area of absence of electrons (positively charged area). From this figure, it can be seen that the HOMO of carnosine is located on the bonds of the imidazole ring of the histidine fragment of the carnosine molecule, on the amino group of the β-alanine fragment, and on the C_{11}-C_{12} bond, with a small amount on the C_{10}-C_{11} and C_6-H_{20} bonds and the nitrogen atom N_9. When transitioning to LUMO, the amino group is completely released, and the electron density is concentrated over the hydrogen atoms H_{19}, H_{18} of the imidazole ring and the H_{23} hydrogen of the peptide bond. A small amount of electron density is localized on the atoms O_{15}, N_9, N_{11}, and on the bond N_1-C_5 of the imidazole ring, while the atoms N_1, C_2, and C_4 of the imidazole ring are united by electron density within the ring. The molecular electrostatic potential (MEP) is considered to be the most informative descriptor. MEP surfaces visualize the three-dimensional charge distribution within a whole molecule. Analysis of the MEP allows predicting the chemical reactivity of the molecule and to determine the sites of ligand binding during complex formation. The MEP is a graph of the dependence of the electrostatic potential plotted on a surface with constant electron density. Fig.6 shows the MEP map of the carnosine molecule. Red and yellow colors indicate areas with low potential, characterized by an abundance of electrons, susceptible to electrophilic attack. Blue color indicates an area with high potential, relatively lacking electrons, this is the area of nucleophilic attack. As we can see, the most active reactive centers of carnosine are the oxygen atoms of the carboxyl and peptide groups; the nitrogen atoms N_1 of the imidazole ring and N_{13} of the amine group can also be subject to electrophilic attack (yellow color). The bright blue color is located above the hydrogen atom H_{18} of the imidazole ring.

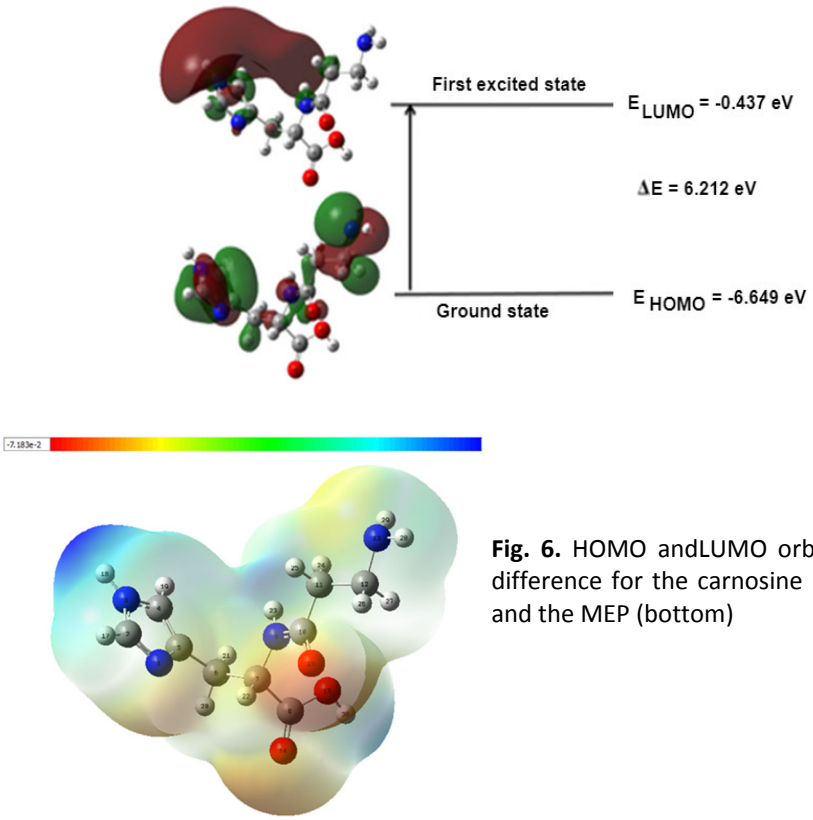

Fig. 6. HOMO andLUMO orbitals and their difference for the carnosine molecule (top) and the MEP (bottom)

Molecular docking

At the next step, which involves the molecular docking procedure, in order to fit the ligand molecule carnosine with the protein 1xbn, the ligand O_2 and all water molecules that could interfere with the step-by-step fitting are preliminarily removed from the structure of the protein 1xbn. Next, the protein is protonated, i.e., the protein structure is supplemented with hydrogen atoms that are absent in the experimental structure. It should also be noted that the docking program does not recognize metal atoms, to which it always assigns a charge of zero. Therefore, to account for the iron atom in the calculation process, a fictitious atom with a charge of +2 was manually introduced into the structure of the complex. Next, the eight torsional rotation angles for the dipeptide are automatically selected.

The resulting structures of the protein and ligand with their assigned charges are saved as the initial working pdbqt files. Then, the dimensions of the hypothetical box are selected, with the center being the active site of the protein. In our case, the coordinates of the center of the box were chosen to be the coordinates of a

dummy Fe atom. Such a hypothetical computational box was represented as a cube with an edge of 18 Å. The box grid was adjusted to allow for a stepwise docking procedure with a step size of 1.0 Å. The optimization of the ligand's position within the protein's active site is carried out based on the results of the binding energy assessment of the ligand with the macromolecule. The energy calculation is performed based on a pre-prepared potential grid. From a mathematical perspective, docking represents the search for the global minimum of the free energy function defined in the multidimensional space of all possible ligand-protein binding modes.According to the study results, the lowest-energy conformational states of the ligand in the active site of the protein correspond to the 9 poses described in Table 3. The results of the docking program include binding energy values ΔG obtained using the gradient descent method. The essence of the method is based on finding the match between the surfaces of the ligand and the protein to achieve the maximum surface area upon their contact.

As follows from the calculation results, the binding energy varies in the range from -4.6 to -1.9 kcal/mol for different positions of carnosine in the active site of the protein. Table 3 also contains the root mean square deviation (R_{msd}) values between the initial position of the ligand in the active site of the protein and the conformation with the local energy minimum after energy minimization, obtained during the search according to the formula:

$$R_{msd} = \sqrt{\frac{\sum_{i=1}^{N} a_i}{N}},$$

where a_i −the distance between the i −th atoms in various positions.

Table 3. Binding energies of carnosine in various positions at the active site of soluble guanylate cyclase 1xbn, predicted by Autodock Vina

Pose	Binding energy, ΔG (kcal/mol)	Distance from the best mode (Å)	
		rmsd l.b.	rmsd u.b.
1	-4.5	0.000	0.000
2	-4.2	2.527	5.275
3	-4.0	16.784	19.168
4	-3.8	2.333	3.581
5	-3.8	17.172	18.867
6	-3.3	16.890	19.041
7	-3.2	16.963	18.506
8	-2.9	13.461	16.426
9	-1.9	17.089	19.233

To visualize the results obtained from the stepwise docking procedure, the AutoDockTools program was used. The program includes a number of methods for analyzing docking simulation results, including tools for clustering results based on conformational similarity, visualizing 9 conformations, and visualizing interactions between the ligand and the protein. The docking process involves prediction of the ligand conformation, description of orientation within this site (referred to as pose), and assessment of the binding affinity. Fig.7 shows the positions of the ligand in the docking box for all nine obtained low-energy docking poses (for clarity, all structures in Fig.7 are shown against the background of the heme as a surface).

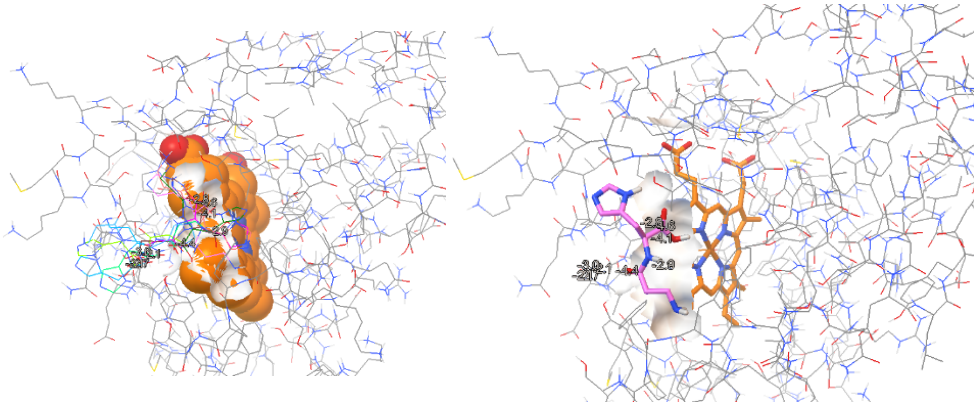

Fig. 7. (a) The heme component of the protein and (b) the structure of carnosine in the active site (various images from the AutoDocTool program).

In Fig.8, the most favorable poses of carnosine are presented, visualized using the graphical program PyMol (heme-carnosine in pose 1).

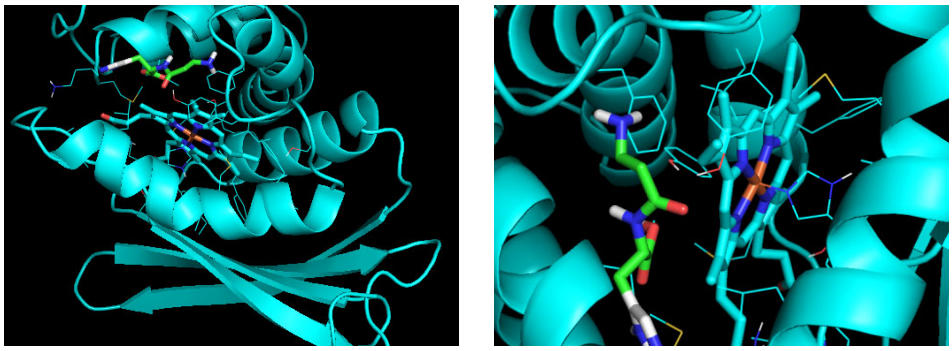

Fig. 8. Guanylate cyclase 1xbn+heme and carnosine in pose 1 (according to PyMol data). On the right, the same image in an enlarged format.

As seen in Fig.8, the heme component of protein and carnosine are located in the binding pocket of the GC and are surrounded on all sides by the main chain of guanylate cyclase 1xbn. The side chains of all amino acid residues located in the active site of the protein within approximately 4Å from the Fe atom are clearly visible. The side chains of the amino acid residues of the protein are shown as solid lines. As seen from Fig.8, the molecule of carnosine, after entering the binding pocket of guanylate cyclase, interacts with the propionyl residues on one side of the heme, preventing further advancement of the ligand deeper into the pocket and depriving it of the ability to interact with the iron atom.

For the convenience of visual analysis, Fig.9 shows an image on a white background indicating the distances between the atoms of the ligand and the heme, as well as the distances to the nearest amino acid residues. For example, the distance between the ligand and the atoms of Tyr 85 was found to be 2.4Å, with Phe78 this distance is 3.6Å, and with the hydroxyl group of Leu105 this distance is 3.7Å. The distance between carnosine and the heme component of guanylate cyclase varies between 3.3-3.6Å.

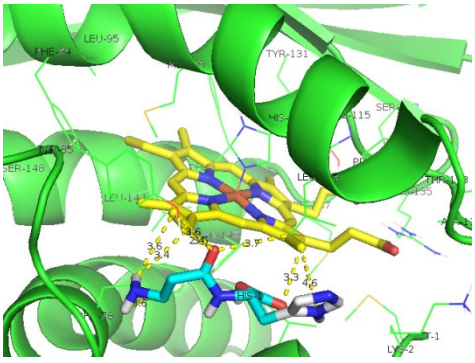

Fig. 9. Guanylate cyclase + heme and carnosine in pose 1. For clarity, the active site is shown on a white background.

The presence of stable interactions between the ligand and the Tyr85 atoms is also confirmed by the results of experimental studies. In the work carried out by the Boon and co-authors [12], it was also shown that presence of a hydrogen-bonding tyrosine residue in the distal pocket of the heme is necessary for for O_2 binding in the H-NOXβ1 subunit family of sGC. Indeed, the removal of the oxygen molecule from the active pocket causes the free tyrosine to participate in intermolecular interactions with carnosine.

Next, we analyze other poses of carnosine in the active center of guanylate cyclase. Fig.10 shows the distances between the atoms of carnosine in pose 2 which involved to interactions with heme atoms, as well as the distances between the atoms of carnosine and the neighboring amino acid residues located in the active center of the protein. In this case, the distance between the ligand and the Tyr 85 atoms is found to be 1.9 Å for the hydroxyl groups (OH…..OH), and the length of the resulting hydrogen bond is 2.3 Å. The distance to the heme component is 2.7 Å,

while to the imidazole atoms this distance increases to 3.9 Å for N…N and to 4.5 Å for O…C.

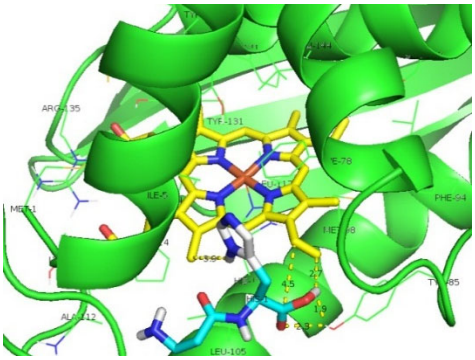

Fig. 10. Active site of guanylate cyclase+ heme and carnosine (pose 2).

Fig. 11 shows the interactions between the atoms of the 3rd binding position of carnosine and the heme atoms of guanylate cyclase.Two different perspectives of the drawings were chosen for a clearer arrangement of the structures and precise determination of the corresponding distances between the atoms of carnosine and the atoms of the heme propionate residues: OH…C = 2.5 Å; O…C = 3.7 Å; O…C = 3.3 Å; O…C = 3.1 Å; O…C = 3.9 Å.

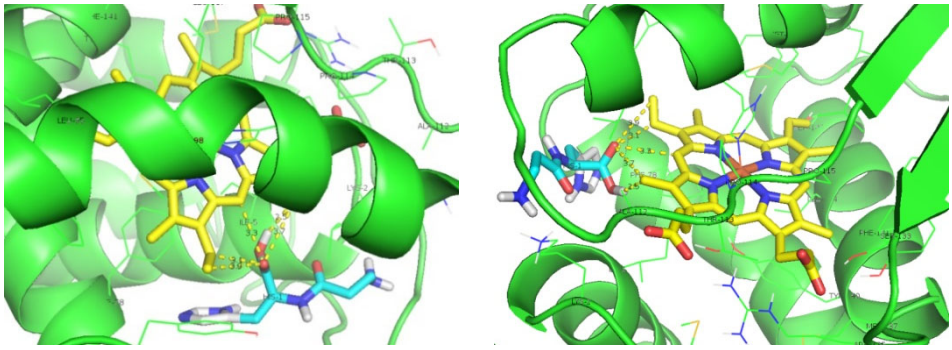

Fig. 11. Active site of guanylate cyclase + heme and carnosine (pose 3). On the right, another angle of the same figure is shown.

3. Conclusion

Summarizing the results of the conducted study, it can be said that the N^1H tautomer of carnosine, used for molecular docking, binds to the active site of guanylate cyclase, forming stable complexes in the region close to the heme pocket, and is characterized by a binding affinity of -4.5 kcal/mol (Table 3). However, to identify the potential for forming more stable bonds between carnosine and the iron atom in the heme pocket of the guanylate cyclase receptor 1xbn, additional studies are

required. These should include the examination of the N^3H tautomer of carnosine and its derivatives, such as anserine and homocarnosine, as well as conducting docking procedures with other known guanylate cyclase structures available in the Protein Data Bank. Based on such comprehensive studies, it will be possible to predict the prospects of using various complexes of carnosine and its analogues as inhibitors of soluble guanylate cyclase for the development of new therapeutic drugs.

References

[1] Frisch M.J. et all. Gaussian 09, Revision D.01, Gaussian, Inc.: Wallingford CT, 2013

[2] Dennington R., Keith T.A., and Millam J.M., GaussView, Version 6.0, Semichem Inc.:Shawnee Mission, KS, 2016.

[3] DeLano W.L. The PyMOL Molecular Graphics System. San Carlos, CA, USA: Delano Scientific, 2002. https://pymol.org

[4] Friebe A., Mergia E., Dangel O., Lange A., and Koesling D. Fatal gastrointestinal obstruction and hypertension in mice lacking nitric oxide-sensitive guanylyl cyclase. Proc. Natl. Acad. Sci. U.S.A., 2007, v.104, no.18, pp. 7699-7704.

[5] Follmann M., Griebenow N., Hahn M.G., Hartung I., Mais F.J., Mittendorf J., Schäfer M., Schirok H., Stasch J.P., Stoll F., Straub A. The chemistry and biology of soluble guanylate cyclase stimulators and activators. Angewandte Chemie Int. Ed., 2013, v.52, iss.36, p. 9442-9462.

[6] Lucas K.A., Pitari G.M., Kazerounian S., Ruiz-Stewart I., Park J., Schulz S., Chepenik K. P., Waldman S.A. Guanylyl cyclases and signaling by cyclic GMP. Pharmacol. Rev., 2000, v.52, no.3. p.375–413.

[7] Friebe A., Koesling D. Regulation of nitric oxide-sensitive guanylyl cyclase. Circ.Res., 2003, v.93, no.2, p.96-105.

[8] Kuhn M. Structure, Regulation, and function of mammalian membrane guanylyl cyclase receptors with a focus on guanylyl cyclase-A. Circ.Res., 2003, v.93, p.700–709.

[9] Montfort W.R., Wales J.A., Weichsel A.. Structure and activation of soluble guanylyl cyclase, the nitric oxide sensor. Antioxidants Redox Signal., 2017, v.26, iss.3, p. 107-121.

[10] Gileadi O. Structures of soluble guanylate cyclase: implications for regulatory mechanisms and drug development. Biochemical Society Transactions, 2014, v.42, no.1, p.108-113.

[11] Shah R.C., Sanker S., Wood K.C., Durgin B.G., Straub A.C. Redox regulation of soluble guanylyl cyclase. Nitric Oxide. 2018, v.76, p.97-104.

[12] Boon E.M., Huang S.H., Marletta M.A. A molecular basis for NO selectivity in soluble guanylate cyclase. Nat Chem Biol., 2005, v.1, no.1, p.53-59.

[13] Ma X., Sayed N., Beuve A., van den Akker F. NO and CO differentially activate soluble guanylyl cyclase via a heme pivot-bend mechanism. EMBO J., .2007, v.26, p.578–588.

[14] Pellicena P., Karow D.S., Boon E.M., Marletta M.A., Kuriyan J. Crystal structure of an

oxygen-binding heme domain related to soluble guanylate cyclases. PNAS., 2004, v.101, iss.35, p.12854-12859.

[15] Derbyshire E.R., Marletta M.A. Structure and regulation of soluble guanylate cyclase. Annu. Rev. Biochem., 2012, v.81, p.533–559.

[16] Kang Y., Liu R., Wu J-X., Chen L. Structural insights into the mechanism of human soluble guanylate cyclase. Nature, 2019, v.574, p.206-210.

[17] Childers K.C., Garcin E.D. Structure/function of the soluble guanylyl cyclase catalytic domain, Nitric Oxide, 2018, v.77, p.53-64.

[18] Montfort W.R., Wales J.A., Weichsel A. Structure and activation of soluble guanylyl cyclase, the nitric oxide sensor. Antioxid Redox Signal. 2017, v.26, no.3, p.107–121.

[19] Allerston C.K., von Delft F., Gileadi O. Crystal structures of the catalytic domain of human soluble guanylate cyclase. PLoS ONE 8, 2013, e57644.

[20] Fritz B.G., Roberts S.A., Ahmed A., Breci L., Li W., Weichsel A., Brailey J.L., Wysocki V.H., Tama F., Montfort W.R. Molecular model of a soluble guanylyl cyclase fragment determined by small-angle X-ray scattering and chemical cross-linking. Biochemistry, 2013, v.52, p.1568-1582.

[21] Wu G., Sharina I., Martin E. Soluble guanylyl cyclase: Molecular basis for ligand selectivity and action in vitro and in vivo. Review article. Front.Mol.Biosci., 2022, Sec. Protein Biochemistry for Basic and Applied Sciences, v.9.

[22] Underbakke E. S. et al. Nitric oxide-induced conformational changes in soluble guanylate cyclase.Structure, 2014, v.22, p.602–611.

[23] Sharina I., Martin E. Cellular factors that shape the activity or function of nitric oxide-stimulated soluble guanylyl cyclase. Cells, 2023, v.12(3), p.471.

[24] Boon E.M., Davis J.H.,Tran R., Karow D.S., Huang S.H., Pan D., Miazgowicz M.M., Mathies R.A., Marletta M.A. Nitric oxide binding to prokaryotic homologs of the soluble guanylate cyclase beta1 H-NOX domain. J.Biol.Chem., 2006, v.281, no.31, p.21892-21902.

[25] Boon E.M., Marletta M.A. Ligand specificity of H-NOX domains: from sGC to bacterial NO sensors. J. Inorg. Biochem., 2005, v.99, no.4, p.892-902.

[26] Evgenov O.V., Pacher P., Schmidt P.M., Haskó G.,Schmidt H.H.,Stasch J.P.NO-independent stimulators and activators of soluble guanylate cyclase: Discovery and therapeutic potential Nat. Rev.Drug Discov., 2006, v.5, p.755-768.

[27] Follmann M., Griebenow N., Hahn M.G., Hartung I., Mais F.J., Mittendorf J., Schäfer M., Schirok H., Stasch J.P., Stoll F., Straub A. The chemistry and biology of soluble guanylate cyclase stimulators and activators Angew. Chem. Int. Ed. Engl, 2013, v.52, p.9442-9462.

[28] Roy B., Garthwaite J. Nitric oxide activation of guanylyl cyclase in cells revisited. Proc.Natl.Acad.USA, 2006, v.103, iss.32, p.12185-12190.

[29] Stasch J.P., Becker E.M., Alonso-Alija C., Apeler H., Dembowsky K., Feurer A., Gerzer R., Minuth T., Perzborn E., Pleiss U., Schröder H., Schroeder W., Stahl E., Steinke W., Straub A., Schramm M. NO-independent regulatory site on soluble guanylate cyclase Nature, 2001, v.410, p.212-215.

[30] Martin E., Berka V., Sharina I., Tsai A.L. Mechanism of binding of NO to soluble guanylyl cyclase: Implication for the second NO binding to the heme proximal site. Biochemistry, 2012, v.51, iss.13, p.2737–2746.

[31] Martin E., Berka V., Tsai A.L., Murad F. Soluble guanylyl cyclase: The nitric oxide receptor. Methods Enzymol., 2005a, v.396, p.478–492.

[32] Russwurm M., Koesling D. NO activation of guanylyl cyclase. Embo J., 2004, v.23, iss.22, p.4443–4450.

[33] Sandner P., Zimmer D.P., Milne G.T., Follmann M., Hobbs A., Stasch J. P. Soluble guanylate cyclase stimulators and activators. Handb. Exp. Pharmacol., 2019, v.264, p.355–394.

[34] Schmidt P., Schramm M., Schroder H., Stasch J.P. Mechanisms of nitric oxide independent activation of soluble guanylyl cyclase. Eur. J. Pharmacol., 2003, v.468, iss.3, p.167–174.

[35] Tsai A.L., Berka V., Sharina I., Martin E. Dynamic ligand exchange in soluble guanylyl cyclase (sGC): Implications for sGC regulation and desensitization. J. Biol. Chem., 2011a, v.286, iss.50, p.43182–43192.

[36] Boon E.M., Huang S.H., Marletta M.A. A molecular basis for NO selectivity in soluble guanylate cyclase. Nat. Chem. Biol., 2005, v.1, no.1, p.53-59.

[37] Ben Aissa M., Tipton A.F., Bertels Z., Gandhi R., Moye L.S., Novack M., Bennett B.M., Wang Y., Litosh V., Lee S.H., Gaisina I.N., Thatcher G.R., Pradhan A.A. Soluble guanylyl cyclase is a critical regulator of migraine-associated pain. Cephalalgia, 2017, v.38, no.8, p. 1471-1484.

[38] Olesen J. Nitric oxide-related drug targets in headache. Neurotherapeutics, 2010, v.7, no.2, p.183-190.

[39] Pyriochou A., Beis D., Koika V., Potytarchou C., Papadimitriou E., Zhou Z., Papapetropoulos A. Soluble guanylyl cyclase activation promotes angiogenesis. J.Pharmacol.Exp.Ther., 2006, v.319, no.2, p.663-671.

[40] Morbidelli L., Pyriochou A., Filippi S., Vasileiadis I., Roussos C., Zhou Z., Loutrari H., Waltenberger J., Stossel A., Giannis A., Ziche M., Papapetropoulos A. The soluble guanylyl cyclase inhibitor NS-2028 reduces vascular endothelial growth factor-induced angiogenesis and permeability. Am.J.Physiol.Regul.Integr.Comp.Physiol., 2010, v.298, p.824–832.

[41] Fraser M., Chan S.L., Chan S.S.L., Fiscus R.R., Tsang B.K.. Regulation of p53 and suppression of apoptosis by the soluble guanylyl cyclase/cGMP pathway in human ovarian cancer cells. Oncogene, 2006, v.25, p.2203-2212.

[42] Fernandes D., Sordi R., Pacheco L.K., Nardi G.M., Heckert B.T., Villela C.G., Lobo A.R., Barja-Fidalgo C., Assreuy J. Late, but not early, inhibition of soluble guanylate cyclase decreases mortality in a rat sepsis model. J.Pharmacol.Exp.Ther., 2009, v.328, no.3, p.991–999.

[43] Tseng K.Y., Caballero A., Dec A., Cass D.K., Simak N., Sunu E., Park M.J., Blume S.R., Sammut S., Park D.J., West A.R.. Inhibition of striatal soluble guanylyl cyclase-cGMP

signaling reverses basal ganglia dysfunction and Akinesia in experimental parkinsonism. PLoS One, 2011, v.6, p.11.

[44] Zhang L., Dawson V.L., Dawson T.M. Role of nitric oxide in Parkinson's disease. Pharmacol. Ther., 2006, v.109. no.1-2, p.33-41.

[45] Ghanta M., Panchanathan E., Lakkakula B.V., Narayanaswamy A. Retrospection on the role of soluble guanylate cyclase in Parkinson's disease. J Pharmacol Pharmacother., 2017, v.8, no.3, p.87-91.

[46] Hipkiss Alan R. Chapter 3: carnosine and its possible roles in nutrition and health. advances in food and nutrition research., 2009, v.57, p.87-154.

[47] Hsieh C.L., Ho Y.C., Lai H.H., Yen G.C. Inhibitory effect of carnosine and anserine on DNA oxidative damage induced by Fe2+, Cu2+ and H2O2 in lymphocytes. Journal of Food and Drug Analysis, 2002, v.10, no.1, p.47-54.

[48] Hipkiss A.R., Baye E., de Courten B. Carnosine and the processes of ageing. Maturitas, 2016, v.93, p.28-33.

[49] Reddy V.P., Garrett M.R., Perry G., Smith M.A. Carnosine: A versatile antioxidant and antiglycating agent (Review). Sci. Aging Knowl. Environ., 2005, v.18, p.12.

[50] Shao L., Li Q.-H., Zheng T. L-Carnosine reduces telomere damage and shortening rate in cultured normal fibroblasts. Biochem.Biophys.Res.Commun., 2004, v.324, no.2, p.931–936.

[51] Gaunitz F., Hipkiss A.R. Carnosine and cancer: a perspective. Amino Acids., 2012, v.43, no.1, p.135-142.

[52] Болдырев А.А. Проблемы и перспективы исследования биологической роли карнозина. Биохимия, 2000, том 65, № 7, с. 884-890

[53] Болдырев А.А. Карнозин. М.: Изд-во МГУ, 1998, 320 с.

[54] Boldyrev A. A., Stvolinsky S. L., Fedorova T. N., Suslina Z. A. Carnosine as a natural antioxidant and geroprotector: From molecular mechanisms to clinical trials. Rejuvenation Research, 2010, v.13, no.2-3, p.156-158.

[55] Lan Shao, Qing-Huan Li, Zheng Tan. L-carnosine reduces telomere damage and shortening rate in cultured normal fibroblasts. Biochem.Bioph.Res.Commun., 2004, v.324, no.2, p.931–936.

[56] Gaunitz F., Hipkiss A.R. Carnosine and cancer: a perspective. Amino Acids., 2012, v.43, no.1, p.135-142.

[57] Riedl E., Pfister F., Braunagel M., Brinkkötter P., Sternik P., Deinzer M., Bakker S.J., Henning R.H., van den Born J., Krämer B.K., Navis G., Hammes H.P., Yard B., Koeppel H. Carnosine prevents apoptosis of glomerular cells and podocyte loss in STZ diabetic rats. Cell Physiol Biochem., 2011, v.28, no.2, p.279-288.

[58] Pfister F., Riedl E., Wang Q., vom Hagen F., Deinzer M., Harmsen M.C., Molema G., Yard B., Feng Y., Hammes H.P. Oral carnosine supplementation prevents vascular damage in experimental diabetic retinopathy. Cell Physiol Biochem., 2011, v.28, no.1, p.125-136.

[59] Rashid I., van Reyk D.M., Davies M.J. Carnosine and its constituents inhibit glycation of low-density lipoproteins that promotes foam cell formation in vitro. FEBS Lett., 2007,

v.58, no.5, p.1067–1070.

[60] Mong M.C., Chao C.Y., Yin M.C. Histidine and carnosine alleviated hepatic steatosis in mice consumed high saturated fat diet. Eur J Pharmacol., 2011, v.653, no.1-3, p.82-88.

[61] Hasanein P., Kazemian-Mahtaj A., Khodadadi I. Bioactive peptide carnosin protects against lead acetate-induced hepatotoxicity by abrogation of oxidative stress in rats. Pharmaceutical Biology, 2016, v.54, no.8, p.1458-1464.

[62] Jun Zhao, Lei Shi, Li-Rong Zhang. Neuroprotective effect of carnosine against salsolinol-induced Parkinson's disease. Exp. Ther. Med., 2017, v.14, no.1, p.664–670.

[63] Demukhamedova S.D., Hajiyev Z.I., Alieva I.N., Godjaev N.M. Theoretical study of carnosine and its derivativies by methods of quantum chemistry and molecular docking // International Congress on carnosine and anserine (ICCA), 12-14 September, 2017 (Louisville, KY,USA)

[64] Demukhamedova S.D., Hajiyev Z.I., Aliyeva I.N., Godjaev N.M. Modeling of the Processes of binding gem-soluble Guanylate Cyclase with Carnosine // 6th International Conference on Control and Optimization with Industrial Applications (COIA-2018), vol.II, p.107-109, 11-13 July, 2018, Baku, Azerbaijan.

[65] Akverdiyeva G.A., Alieva I.N., Hajiyev Z.I., Demukhamedova S.D. Conformational profiles of carnosine // The 7th International Conference on Control and Optimization with Industrial Applications (COIA-2020), 26-28 August 2020, Baku Azerbaijan.

[66] Akverdiyeva G.A., Alieva I.N., Hajiyev Z.I., Demukhamedova S.D. Spatial structure of N1H and N3H tautomers of carnosine in zwitterion form. Journal of Physics (AJP Fizika), 2021, v.XXVII, no.2, p.29-37.

[67] Morris G.M., Huey R., Lindstrom W., Sanner M.F., Belew R.K., Goodsell D.S., Olson A.J. AutoDock4 and AutoDockTools4: Automated docking with selective receptor flexibility. J. Comput. Chem., 2009, v.30, no.16, p.2785–2791.

[68] Trott O., Olson A.J. AutoDock Vina: improving the speed and accuracy of docking with a new scoring function, efficient optimization, and multithreading. Journal of Computational Chemistry, 2010, v.31, no.2, p.455–461.

[69] Nioche P., Raman C.S. Crystal structure of a bacterial nitric oxide sensor: an ortholog of mammalian soluble guanylate cyclase heme domain, 2004, https://www.rcsb.org/

[70] Petersson G.A., Allaham M.A. A complete basis set model chemistry. II. Open-shell systems and the total energies of the first-row atoms. J.Chem.Phys., 1991, v.94, p. 6081-6090.

[71] Wiberg K.B., Rablen P.R. Atomic charges. J.Org. Chem., 2018, v.83, p.15463-15469.

[72] Fukui K. Role of frontier orbitals in chemical reactions. Science, 1982, v.218, p.747-754.

[73] Koopmans T.A. Ordering of wave functions and eigenvalues to the individual electrons of an atom. Physica, 1934, v.1, p.104-113.

[74] Schüürmann G. Quantum chemical descriptors in structure-activity relationships–calculation,interpretation and comparison of methods in predicting chemical toxicity and fate, cronin, M.T.D.; Livingstone, D.J. (Eds.), CRC Press: Boca Raton, FL, 2004, p.85-149.

[75] Perdew J.P., Parr R.G., Levy M., Balduz J.L. Density-functional theory for fractional particle number: Derivative discontinuities of the energy. Phys.Rev.Lett., 1982, v.49, p.1691-1694.

[76] Vasilescu D., Adrian-Scotto M. From Democritus to Schrodinger: A reflection on quantum molecular modeling. Struct. Chem., 2010, v.21, p.1289-1314.

[77] Geerlings P., De Proft F., Langenaeker W. Conceptual density functional theory. Chem. Rev., 2003, v.103, p.1793-1873.

[78] Parr R.G., Pearson R.G. Absolute hardness: Companion parameter to absolute electronegativity. J. Amer. Chem. Soc., 1983, v.105, p.7512-7516.

[79] Senet P. Chemical hardnesses of atoms and molecules from frontier orbitals. Chem.Phys. Lett.,1997, v.275, p.527-532.

[80] Parr R.G., Szentpaly L., Liu S. Electrophilicity index. J.Amer.Chem.Soc., 1999, v.121, p.1922-1924.

[81] Parthasarathi P., Subramanian V., Roy D.R., Chattaraj P.K. Electrophilicity index as a possible descriptor of biological activity. Bioorg. Med. Chem., 2004, v.12, p.5533-5543.